

Shaping non-reciprocal caustic spin-wave beams

Dinesh Wagle,¹ Daniel Stoeffler,² Loic Temdie,³ Mojtaba Taghipour Kaffash,¹ Vincent Castel,³ Hicham Majjad,² Romain Bernard,² Yves Henry,² Matthieu Bailleul,² M. Benjamin Jungfleisch,^{1,*} and Vincent Vlaminck^{3,†}

¹*Department of Physics and Astronomy, University of Delaware, Newark, DE 19716, USA*

²*IPCMS - UMR 7504 CNRS Institut de Physique et Chimie des Matériaux de Strasbourg, France*

³*IMT- Atlantique, Dpt. MO, Lab-STICC - UMR 6285 CNRS, Technopole Brest-Iroise CS83818, 29238 Brest Cedex 03, France*

(Dated: December 20, 2024)

Caustics are intricate and challenging to control near-field interference patterns that exist in a wide range of physical system, and which usually exhibit a reciprocal wave propagation. Here, we utilize the highly anisotropic dispersion and inherent non-reciprocity of a magnonic system to shape non-reciprocal emission of caustic-like spin wave beams in an extended 200 nm thick yttrium iron garnet (YIG) film from a nano-constricted *rf* waveguide. We introduce a near-field diffraction model to study spin-wave beamforming in homogeneous in-plane magnetized thin films, and reveal the propagation of non-reciprocal spin-wave beams directly emitted from the nanoconstriction by spatially resolved micro-focused Brillouin light spectroscopy (BLS). The experimental results agree well with both micromagnetic simulation, and the near-field diffraction model. The proposed method can be readily implemented to study spin-wave interference at the sub-micron scale, which is central to the development of wave-based computing applications and magnonic devices.

Caustics is a commonly used term to describe concentration of wave intensity influenced by curvilinear landscape of diffusion or emission. They have been a subject of curiosity in a variety of physical systems, ranging from optics [1] and dark matter physics [2, 3] to condensed matter physics, including phononics [4–6], plasmonics [7, 8], electronics [9–11], and magnonics [12–23]. While the concept of caustics in optics refers to the concentration of light rays due to reflection or refraction within a heterogeneous system, caustic beams in condensed matter physics are related to the anisotropy of the dispersion relation in a homogeneous system, where the direction of the group velocity and wavevector do not coincide. More specifically, the existence of inflection points in the isofrequency curve of an anisotropic system leads to a range of wavevectors with group velocity pointing in the same direction. This low spread in group velocity directions around these inflection points results in the generation of a caustic beam.

In the last decade, caustics in spin systems have been extensively studied theoretically [12, 13, 23, 24], and experimentally for their advantages with respect to the development of wave-based computing applications such as reservoir computing [25–27], holographic memory [28, 29], and neuromorphic computing [30, 31]. They appear as a promising effect to shape and steer well-defined spin-wave beams in adjustable frequency bands, and with a higher power density than conventional plane waves. The most established technique to excite well-defined caustic beams is to launch spin waves in a narrow ferromagnetic waveguide that enters a semi-infinite plane [14, 15], where the junction acts as a point-like diffracting source. Other methods to create spin-wave caustics include the utilization of a collapsing bullet mode [16], nonlinear higher harmonic generation from localized edge modes [17], or

are based on all-optical point-like sources based on frequency comb rapid demagnetization [21]. Recently, the excitation of spin-wave caustics has been achieved in extended films from the edges of a straight segment via NV magnetometry [32], using a periodic diffraction grating [33], or in a circular stripline antenna in both the Damon-Eshbach [23], and the backward-volume wave geometry [19]. However, the unique potential of magnonic systems to combine non-reciprocity with nanoscale spin-wave beam shaping in an extended thin film remains to be demonstrated.

Here, we show the non-reciprocal emission of caustic spin-wave beams in an extended yttrium iron garnet (YIG) film from a nano-constricted *rf* waveguide. We extend the previously developed near-field diffraction model (NFD) of spin waves in out-of-plane magnetized films [34, 35] to in-plane magnetized films, which we use to identify suitable antenna designs for shaping spin-wave caustic beams. The predictions are then experimentally tested using micro-focused Brillouin light scattering (BLS) by mapping the spin-wave beam emission. Our experiments reveal a non-reciprocity in the caustic emission that depends on the relative orientation between microwave and biasing magnetic fields. The experimentally obtained spin-wave maps agree well with NFD modeling and micromagnetic simulations. Our results highlight the possibility to control the shaping and steering of spin-wave caustic beams, which feature narrow adjustable bandwidth, and long-range propagation.

Experimentally, the excitation of coherent spin-waves is achieved within a range of wavevector for which the dynamic dipolar interaction usually plays a major role (e.g. $k \leq 100$ rad/ μm). For thin films magnetized in-plane, it is specifically this dipolar term that leads to an anisotropic dispersion relation, where the frequency of

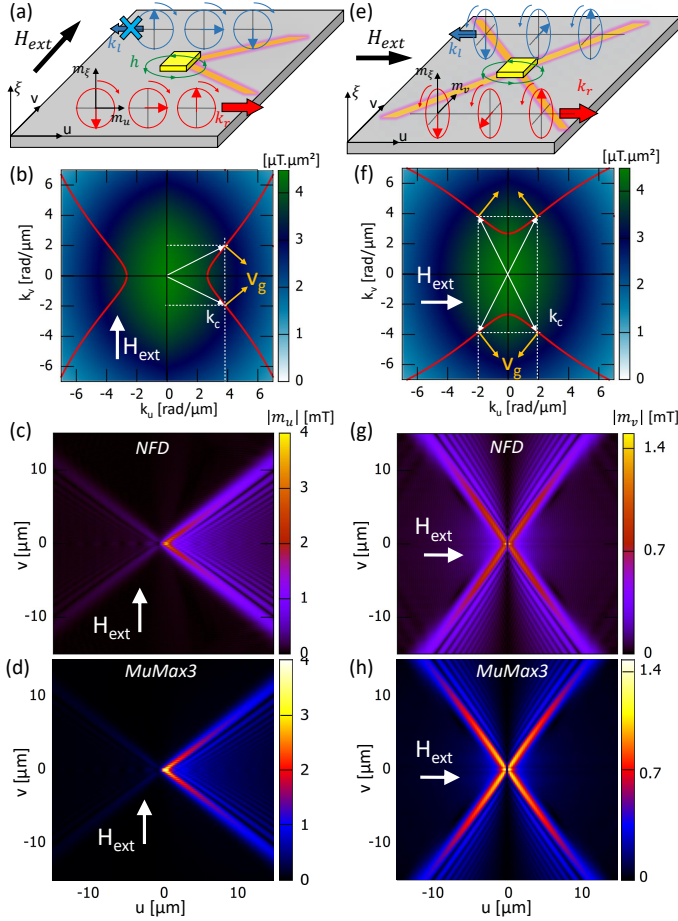


FIG. 1. (a) Sketch of spin wave profile illustrating the chiral coupling in DE-configuration. (b) Isofrequency curve (red) at 7.9 GHz for a 50 nm thick YIG film magnetized along v -axis under a bias field of 200 mT, superimposed with the FFT of the excitation field for a 500 nm square segment. (c) MuMax3, and (d) NFD simulations in the DE-configuration. (e) and (f) Same as (a) and (b) for bias field along u -axis. (g) MuMax3, and (h) NFD simulations in the BVW-configuration.

the spin wave, among other parameters, depends on the relative orientation between magnetization and wavevector [36]. For suitable combinations of field, frequency and wavevector, the isofrequency curve in reciprocal space (k_u, k_v) possesses an inflection point k_c , which is referred to as a caustic point $\frac{d^2 k_u}{dk_u^2}|_{k=k_c} = 0$. In the vicinity of this point k_c of zero curvature, a finite range of wavevectors have a group velocity pointing in the same direction [$\vec{v}_g = \vec{\nabla}_k(\omega)$], which can lead to the emission of a spin-wave caustic beam. The larger the region where the condition $\frac{d^2 k_v}{dk_u^2} \approx 0$ extends, the easier it will be to excite the caustic beams. Another requirement for caustic beam formation besides the aforementioned conditions is a sufficiently constrained (ideally point-like) spin-wave source. Figure 1(a) shows the isofrequency curve at 7.9 GHz for a 50 nm-thick YIG film magnetized along the y -axis by a bias field of 200 mT, on top of which we superimpose the

Fourier transform of the excitation field from a 500 nm square [Fig. 1(a) and (d)] spin-wave source. One can see the necessary condition of having the caustic point located within an effective region of the 2D emission spectrum in order to generate well-defined beams; see also SM for the comparison with a rectangular segment.

In the following, we adapt the NFD approach, which was shown to benchmark spin-wave diffraction in out-of-plane magnetized films [34], for investigating the beamforming in in-plane configurations. The approach consists of defining the dynamic susceptibility tensor $\bar{\chi}_{xy}$ in reciprocal space, which is obtained by inverting the linearized Landau-Lifschitz-Gilbert (LLG) equation [37, 38] in the 2D-frame (x, y) transverse to the bias field direction (z). For simplicity, we ignore magneto-crystalline anisotropy, and consider unpinned conditions [$(\frac{\partial \vec{m}}{\partial \xi})_{\pm t/2} = \vec{0}$] at both top and bottom surfaces. We also restrict ourselves to the fundamental mode ($n = 0$), for which the spin-wave profile is uniform across the thickness, and assume no coupling with higher-order modes. This last assumption is all the more relevant, the thinner the film is, for which higher-order modes are fairly decoupled.

The diffraction pattern from an arbitrarily shaped coplanar waveguide (CPW) can then be obtained by computing the inverse Fourier transform of the matrix product of the susceptibility tensor with the Fourier transform of the excitation field:

$$\vec{m}(u, v, t) = e^{i\omega t} \iint_{-\infty}^{+\infty} dk_u dk_v \bar{\chi} \vec{h}(k_u, k_v) e^{-i(k_u u + k_v v)}. \quad (1)$$

where the susceptibility tensor $\bar{\chi}$, and the excitation field $\vec{h}(k_u, k_v)$ have been expressed in the lab frame (u, v) , which is related to the shape of the spin-wave antenna (cf supplementary material for further details). $\vec{h}(k_u, k_v)$ is a 2-dimensional vector, made of the out-of-plane component h_ξ , and the in-plane component h_{in} transverse to the bias field direction (z). Thus, we obtain a mapping in the steady state of the dynamic magnetization vector $\vec{m}(u, v, t) = (m_\xi, m_{in})$.

Figure 1 shows the spin-wave diffraction patterns obtained for the 500 nm square segment on top of a 50 nm-thick YIG film with a Gilbert damping $\alpha = 2 \times 10^{-4}$. In these simulations, we used a simple excitation profile derived from the expressions of the Oersted field of a 80 nm-thick straight rectangular conductor carrying uniform current density along v , for which we adjusted the current value to have maximum field of 0.1 mT. We simulate two limiting cases: (1) when the bias field is perpendicular to the in-plane component of the excitation field [Fig. 1(c), ‘‘Damon-Eshbach’’-like (DE) configuration], and (2) when the bias field is parallel to the in-plane component of the excitation [(Fig. 1(g), ‘‘backward volume wave’’-like (BVW) configuration)]. Alongside the NFD mapping, we also show in Figs. 1(d),(h) the corresponding micromagnetic simulations using MuMax3, and

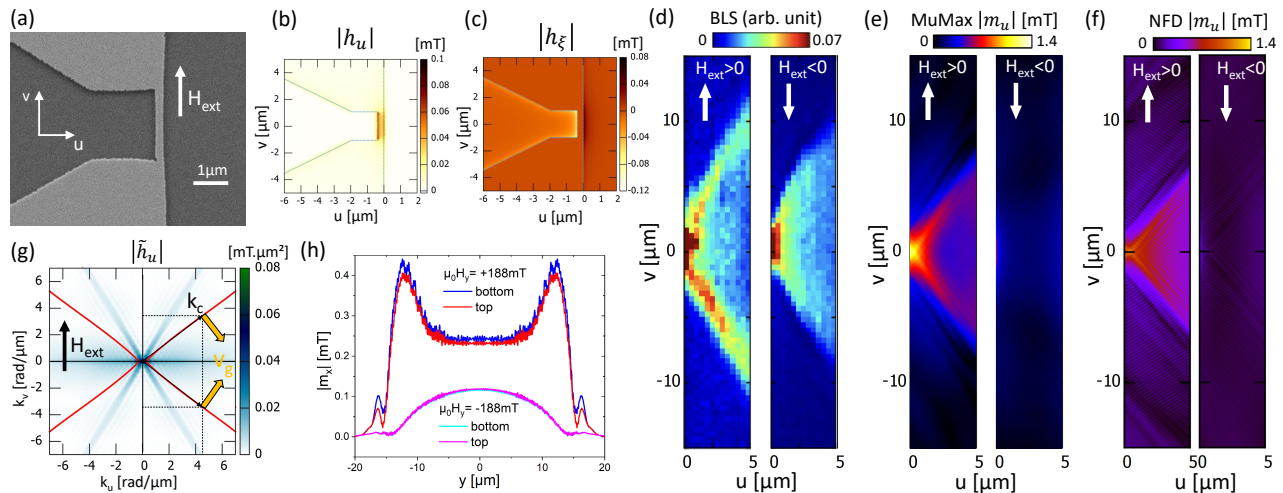


FIG. 2. (a) Scanning microscope image of a 400 nm-wide and 2 μm -long constricted stripline. (b) 2D-field distribution of the in-plane h_u , and (c) out-of-plane h_ξ components of the excitation field obtained via Comsol Multiphysics. (d) BLS measurement at 7.5 GHz, and a bias field $\mu_0 H_{\text{ext}} = \pm 188$ mT applied in the v -direction. (e) Corresponding MuMax3 simulations for the top cell for both bias field polarities, and (f) corresponding NFD simulations. $v = 0$ corresponds to the position of the constriction in (d-f). (g) Superposition of the isofrequency, and the FFT of h_u indicating the effective caustic locations. (h) Cross-section along the v -axis of the spin-wave amplitude $|m_u|$ at $u = 10 \mu\text{m}$ for the top and bottom cells in the MuMax3 simulations for both field polarities.

taking into account the same set of parameters and excitation geometry. We used a $41.6 \times 41.6 \mu\text{m}^2$ window discretized in $(16.6)^3 \text{ nm}^3$ cells having a 6.7 microm large absorbing contour within which the Gilbert damping increases gradually to 0.1 in order to avoid reflections. All MuMax simulations show the steady state amplitude of the dynamic magnetization.

One can clearly appreciate the excellent quantitative agreement between both methods, even in the smallest details of the diffraction pattern. We note that the computing resources needed for a NFD mapping are negligible compared with its corresponding micromagnetic simulations, and hence, these simple tests validate the NFD approach for sufficiently thin in-plane magnetized films. By comparing the two constriction configurations, the 5 μm -long rectangular segment (see SM) and the 500 nm square, we evidence how a point-like source is essential for properly shaping a single caustic beam. Furthermore, a pronounced non-reciprocity is observed in the DE-like configuration, for which drastically reduced intensity is found on the left-hand side with respect to the bias field direction [Figs. 1(c,d)]. As is sketched in Fig. 1(a), a chiral coupling occurs, in which the microwave field distribution only matches the phase profile of spin-waves for a single-sided propagation; also known as the Damon-Eshbach product rule $\vec{k}_\perp / k_\perp = \vec{n}_0 \times \vec{M} / M_s$ [39], where n_0 is the internal normal to the film top surface. This non-reciprocity is all the more effective that the thickness/width aspect ratio of the stripline is close to 1 [40, 41]. In contrast, the caustic beams appear fully symmetrical on either side of the bias field when it is parallel

to the in-plane dynamic field [Figs. 1(g,h)], as both propagation directions are compatible with the out-of-plane microwave field as sketched in Figs. 1(e).

To confirm our theoretical modeling results, we experimentally investigate the generation of caustic beams from a nano-constricted stripline patterned on top of an extended 200-nm thick single-crystal YIG film by micro-focused BLS spectroscopy (see SM for details). We fabricated two sets of antenna to study the two different field orientations: (1) DE-like configuration (Fig. 2), and (2) BVW-like configuration (Fig. 3). Figure 2(a) shows an exemplary scanning electron image of a $L = 2 \mu\text{m}$ -long and $w = 400$ nm-wide constriction patterned on the top of the YIG film, using electron beam lithography followed by ebeam-evaporation of 6-nm Ti/80-nm Au.

(1) Damon-Eshbach-like configuration: We first present the BLS measurement for the geometry where the preponderant in-plane component of the excitation field h_u at the concentration is perpendicular to the static applied field. Figure 2(d) shows the 2D BLS maps obtained for antenna design (A) carrying a continuous microwave power of -3 dBm at 7.5 GHz and an applied field of $\mu_0 H_{\text{ext}} = \pm 188$ mT. Only measurement on the right-hand side of the constriction were achievable as the BLS laser beam cannot penetrate through the gold antenna covering the left handside. For the positive polarity, e.g., field pointing upward [left panel of Fig. 2(d)], we observe two well-defined beams propagating symmetrically away from the constriction at about 58° with respect to the x -axis. Conversely, for the negative polarity, e.g., field pointing downward [right panel of Fig. 2(d)], the beams

are much less defined, and the signal rapidly decays as we move away from the constriction. This field-orientation non-reciprocity is due to the chiral coupling explained above in Fig. 1(a) [40, 41], for which only one propagation direction corresponds to a dynamic magnetization profile matching with the microwave field. This effect appears more pronounced in the corresponding MuMax3 and NFD simulations, shown respectively in Fig. 2(e) and Fig. 2(f), for which we used the microwave field distribution obtained with Comsol Multiphysics as input (see SM for further details). We show the in-plane h_u , and the out-of-plane h_ξ components of the microwave magnetic field in Fig. 2(b), and (c). These differences in chiral coupling between measurement and simulation could be due to the difficulty of defining the microwave field distribution of the real device. Despite these differences, a reasonable agreement between BLS measurements and simulations is found, demonstrating the control of caustic spin-wave beam excitation at the nanoscale directly from an antenna. Fig. 2(g) shows the overlaying of the isofrequency curve at a biasing field of 188 mT with the FFT of the u -component of the microwave magnetic field indicating where the caustic emission k_C is located. We also show in Fig. 2(h) a cross-section along the v -axis of the spin-wave amplitude at $u=10 \mu\text{m}$ for the top and bottom cells of the MuMax3 simulations, which reveals a slightly larger beam amplitude at the bottom surface, although the excitation field decreases by about a factor 2 across the thickness. This is related to the beam localization, which is opposite to the Damon-Eshbach product rule, namely, $\vec{k}_\perp/k_\perp = -\vec{n}_0 \times \vec{M}/M_s$, where n_0 is the internal normal to the film surfaces, consistently with the observations reported on mode profiles of dipole-exchange spin waves [42, 43].

(2) Backward-volume-wave-like configuration:

In this configuration, the bias field is parallel to the in-plane component h_u of the microwave magnetic field at the constriction. Figure 3(a) shows 2D BLS maps obtained for antenna structure (A). The results were obtained using identical experimental conditions as in the DE-configuration, e.g., an excitation frequency of 7.5 GHz, and an external field of $\mu_0 H_{\text{ext}} = \pm 188 \text{ mT}$. As is evident from the figure, a drastically different behavior is observed in the BVW-configuration. Strikingly, the BLS measurements show a single sharply defined caustic beam emitted from the constriction, which exhibits a non-reciprocal behavior upon bias magnetic field reversal. If the magnetic field is positive along the u -axis [$H_{\text{ext}} > 0$, left panel of Fig. 3(a)], a single spin-wave beam propagating in the negative v -direction (downward) is detected. On the other hand, when $H_{\text{ext}} < 0$ [right panel of Fig. 3(a)], a single upward propagating spin-wave beam is detected. Each beam is comparable in intensity, and both have similar caustic angles $\approx \pm 45^\circ$. We show the corresponding MuMax3 and NFD simulations in Fig. 3(b) and Fig. 3(c) for

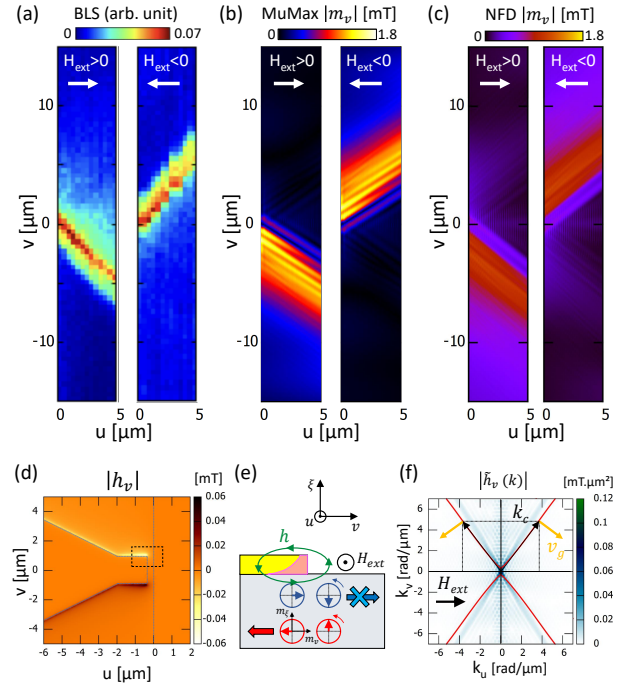


FIG. 3. (a) BLS measurement on a (A)-type device [see Fig. 2(d)] at 7.5 GHz, and a +188 mT (left) and -188 mT (right) bias field applied along u . (b) Corresponding MuMax3, and (c) NFD simulations for both bias field polarities. (d) In-plane v -component of the microwave field obtained with Comsol Multiphysics. (e) Sketch of the chiral coupling occurring at the edges of the constriction in the BVW-configuration. (f) Superposition of the isofrequency and the FFT of the v -component of the microwave field indicating the effecting caustic locations.

which we also used the microwave field distribution obtained via Comsol. Both simulations exhibit similar field-dependent single beam emission (see SM for full scale simulations).

We again attribute this field-dependent non-reciprocity in the BVW-configuration to a chiral coupling, but involving this time the interplay between the out-of-plane ξ -component and the in-plane v -component of the microwave field. As shown in Fig. 3(d), the Comsol simulation reveals that a significant microwave power localized around the edges of the coplanar waveguide, which creates a thin line of in-plane microwave field h_v perpendicular to the bias field close to the constriction. In a similar fashion as in Fig. 1(a), we sketched in Fig. 3(e) the essence of the chiral coupling in this configuration (bias field in the u -direction), where the transverse propagation of a spin-wave in the v -direction is only allowed on the right-hand side of the bias field. We also show in Fig. 3(f) the overlaying of the isofrequency with the FFT of the v -component of the microwave field suggesting better excitation efficiency at the caustic locations compared with the DE configuration shown in

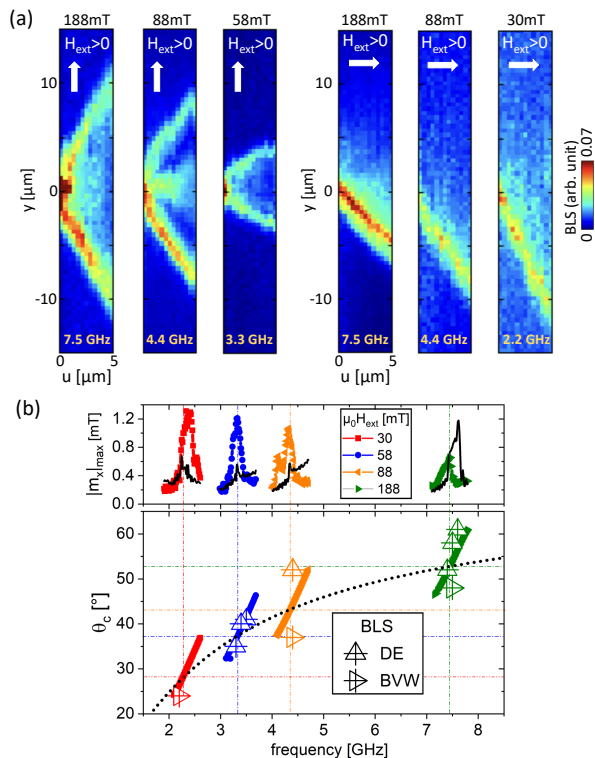


FIG. 4. (a) BLS measurement showing the angular dependence of the field and frequency for a (A)-type constriction. (b) Summary of caustic existence conditions showing: (top panel) the frequency dependence of amplitude $|m_x|_{\max}$, which corresponds to the maximum amplitude of $|m_x|$ at $x=10\ \mu\text{m}$ in the NFD simulations (black lines correspond to BVW-configuration, colored lines correspond to DE-configuration), and (bottom panel) the caustic angle $\theta_c = \pi/2 - (\vec{v}_g, \vec{H}_{\text{ext}})$. (black dashed line) Caustic angle at field and frequency of FMR, extracted from the isofrequency curve.

Fig. 2(g) [evidenced by a closer overlap of the microwave magnetic field strength (color plot) and the isofrequency curve (red line)]. Besides the satisfying agreement between measurement and simulations, one notices that the measured beam appears slightly thinner than in the simulations, which is likely due to the difficulty of reproducing the microwave field distribution of the real device.

In the following, we analyze the angular dependence of the beam formation as a function of the bias field and excitation frequency, as well as the frequency dependence of the beam intensity at a given field. Figure 4(a) shows 2D BLS maps at several bias fields (188, 88, 58, 30) mT, respectively at (7.5, 4.4, 3.3, 2.2) GHz for both configurations. We observe that the beams can be gradually steered toward the equilibrium direction as the frequency is increased. In the DE-like configuration, the angle of the caustic beam with respect to the u -axis increases with frequency, while in the BVW-like configuration (field pointing along the u -axis), the angle decreases

with increasing frequency. Figure 4(b) compares the experimentally obtained angles with the theoretically expected caustic angles, derived numerically from $f(k_u, k_v)$ as the angle between the group velocity and the direction perpendicular to the bias field. We find a reasonable agreement within the error bars for the DE-like configuration, while the measured angles are systematically lower than the theoretically expected ones for the BVW-like configuration.

Additionally, we performed 50 NFD simulations for each bias field value over a 700 MHz frequency span to plot the frequency dependence of the caustic-beam amplitude, as presented in the upper panel of Fig. 4(b). Strikingly, we find that the caustic-beam amplitude peaked right around the field-frequency value corresponding to the ferromagnetic resonance (FMR) condition. This observation is consistent with the fact that the zero curvature ($d^2k_v/dk_u^2 \sim 0$) of the isofrequency curve extends over a broader range of wavevectors at around the FMR frequency for a given field. Furthermore, one notices that the peak amplitude of the caustic beams decreases with frequencies in the DE-configuration whereas it increases in the BVW-configuration [compare black and colored lines in the top panel of Fig. 4(b)].

In conclusion, we demonstrated theoretically and experimentally the possibility to shape non-reciprocal caustic beams in homogeneous ferromagnetic thin film directly from a nano-constricted stripline. Firstly, we introduced a model that efficiently and accurately predicts spin-wave diffraction in thin film magnetized in-plane, and which can readily predict the shaping of caustic spin-wave beams from arbitrary shaped antenna. Then, using microfocused BLS, we confirmed the predictions of the model, revealing spin-wave caustic chiral emission from nanometric constrictions. We studied two measurement configurations, one for which the in-plane microwave field was essentially perpendicular to the magnetization (DE) throughout the constriction, and the other one for which they were parallel to each other (BVW). In the DE configuration, we observed a chiral excitation of two spin-wave beams for a given field polarity. In the BVW configuration, we observed a single non-reciprocal upward- or downward-going beam that can be controlled at ease by changing the polarity of the bias field, and with a steerability precisely controlled by tuning the bias field magnitude and the excitation frequency. Our work provides deep insight into tailoring spin-wave caustics using nano-sized waveguides, which we expect will accelerate the development of interference-based magnonic logic and computing devices.

The authors would like to acknowledge the financial support from the French National research agency under the project *MagFunc*/ANR-20-CE91-0005, the Département du Finistère through the project *SOSMAG*, and the Transatlantic Research Partnership, a program

of FACE Foundation and the French Embassy. We also acknowledge financial support by the Interdisciplinary Thematic Institute QMat, as part of the ITI 2021-2028 Program of the University of Strasbourg, CNRS and Inserm, IdEx Unistra (ANR 10 IDEX 0002), SFRI STRAT'US Project (ANR 20 SFRI 0012) and ANR-17-EURE-0024 under the framework of the French Investments for the Future Program, as well as the High Performance Computing Center of the University of Strasbourg for supporting this work by providing scientific support and access to computing resources. Part of the computing resources were funded by the Equipex Equip@Meso project (Programme Investissements d'Avenir) and the CPER Alsacalcul/Big Data. Research at the University of Delaware was supported by the U.S. Department of Energy, Office of Basic Energy Sciences, Division of Materials Sciences and Engineering under Award DE-SC0020308. The authors acknowledge the use of facilities and instrumentation supported by NSF through the University of Delaware Materials Research Science and Engineering Center, DMR-2011824. We thank Anish Rai for characterizing the YIG films by FMR.

* mbj@udel.edu

† vincent.vlaminck@imt-atlantique.fr

- [1] Y. A. Kravtsov and Y. I. Orlov, *Caustics, Catastrophes and Wave Fields* (Springer Berlin Heidelberg, 1993).
- [2] D. Davydov and S. Troitsky, Testing universal dark-matter caustic rings with galactic rotation curves, *Physics Letters B* **839**, 137798 (2023).
- [3] S. D. M. White and M. Vogelsberger, Dark matter caustics, *Monthly Notices of the Royal Astronomical Society* **392**, 281 (2009).
- [4] A. G. Every, Formation of phonon-focusing caustics in crystals, *Physical Review B* **34**, 2852 (1986).
- [5] H. J. Maris, Enhancement of heat pulses in crystals due to elastic anisotropy, *The Journal of the Acoustical Society of America* **50**, 812–818 (1971).
- [6] B. Taylor, H. J. Maris, and C. Elbaum, Phonon focusing in solids, *Physical Review Letters* **23**, 416–419 (1969).
- [7] X. Shi, X. Lin, F. Gao, H. Xu, Z. Yang, and B. Zhang, Caustic graphene plasmons with Kelvin angle, *Physical Review B* **92**, 081404 (2015).
- [8] I. Epstein and A. Arie, Arbitrary bending plasmonic light waves, *Physical Review Letters* **112**, 023903 (2014).
- [9] J. Spector, H. L. Stormer, K. W. Baldwin, L. N. Pfeiffer, and K. W. West, Electron focusing in two-dimensional systems by means of an electrostatic lens, *Applied Physics Letters* **56**, 1290–1292 (1990).
- [10] V. V. Cheianov, V. Fal'ko, and B. L. Altshuler, The focusing of electron flow and a veselago lens in graphene p-n junctions, *Science* **315**, 1252–1255 (2007).
- [11] J. Cserti, A. Pályi, and C. Péterfalvi, Caustics due to a negative refractive index in circular graphene junctions, *Physical Review Letters* **99**, 10.1103/physrevlett.99.246801 (2007).
- [12] O. Büttner, M. Bauer, S. O. Demokritov, B. Hillebrands, Y. S. Kivshar, V. Grimalsky, Y. Rapoport, and A. N. Slavin, Linear and nonlinear diffraction of dipolar spin waves in yttrium iron garnet films observed by space- and time-resolved brillouin light scattering, *Physical Review B* **61**, 11576–11587 (2000).
- [13] V. Veerakumar and R. E. Camley, Magnon focusing in thin ferromagnetic films, *Physical Review B* **74** (2006).
- [14] V. E. Demidov, S. O. Demokritov, D. Birt, B. O'Gorman, M. Tsoi, and X. Li, Radiation of spin waves from the open end of a microscopic magnetic-film waveguide, *Physical Review B* **80** (2009).
- [15] T. Schneider, A. A. Serga, A. V. Chumak, C. W. Sandweg, S. Trudel, S. Wolff, M. P. Kostylev, V. S. Tiberkevich, A. N. Slavin, and B. Hillebrands, Non-diffractive subwavelength wave beams in a medium with externally controlled anisotropy, *Physical Review Letters* **104** (2010).
- [16] M. P. Kostylev, A. A. Serga, and B. Hillebrands, Radiation of caustic beams from a collapsing bullet, *Physical Review Letters* **106**, 134101 (2011).
- [17] T. Sebastian, T. Brächer, P. Pirro, A. A. Serga, B. Hillebrands, T. Kubota, H. Naganuma, M. Oogane, and Y. Ando, Nonlinear emission of spin-wave caustics from an edge mode of a microstructured $\text{Co}_2\text{Mn}_{0.6}\text{Fe}_{0.4}\text{Si}$ waveguide, *Physical Review Letters* **110**, 067201 (2013).
- [18] R. Gieniusz, H. Ulrichs, V. D. Bessonov, U. Guzowska, A. I. Stognii, and A. Maziewski, Single antidot as a passive way to create caustic spin-wave beams in yttrium iron garnet films, *Applied Physics Letters* **102**, 102409 (2013).
- [19] M. Madami, Y. Khivintsev, G. Gubbiotti, G. Dudko, A. Kozhevnikov, V. Sakharov, A. Stal'makhov, A. Khitun, and Y. Filimonov, Nonreciprocity of backward volume spin wave beams excited by the curved focusing transducer, *Applied Physics Letters* **113** (2018).
- [20] Y. Shiota, S. Funada, R. Hisatomi, T. Moriyama, and T. Ono, Imaging of caustic-like spin wave beams using optical heterodyne detection, *Applied Physics Letters* **116**, 192411 (2020).
- [21] S. Muralidhar, R. Khymyn, A. A. Awad, A. Alemán, D. Hanstorp, and J. Åkerman, Femtosecond laser pulse driven caustic spin wave beams, *Physical Review Letters* **126**, 037204 (2021).
- [22] R. A. Gallardo, P. Alvarado-Seguel, A. Kákay, J. Lindner, and P. Landeros, Spin-wave focusing induced by dipole-dipole interaction in synthetic antiferromagnets, *Physical Review B* **104** (2021).
- [23] A. Wartelle, F. Vilsmeier, T. Taniguchi, and C. H. Back, Caustic spin wave beams in soft thin films: Properties and classification, *Phys. Rev. B* **107**, 144431 (2023).
- [24] J.-V. Kim, R. L. Stamps, and R. E. Camley, Spin wave power flow and caustics in ultrathin ferromagnets with the dzyaloshinskii-moriya interaction, *Physical Review Letters* **117**, 10.1103/physrevlett.117.197204 (2016).
- [25] A. Papp, G. Csaba, and W. Porod, Characterization of nonlinear spin-wave interference by reservoir-computing metrics, *Applied Physics Letters* **119**, 112403 (2021).
- [26] M.-K. Lee and M. Mochizuki, Reservoir computing with spin waves in a skyrmion crystal, *Physical Review Applied* **18** (2022).
- [27] O. Lee, T. Wei, K. D. Stenning, J. C. Gartside, D. Prestwood, S. Seki, A. Aqeel, K. Karube, N. Kanazawa, Y. Taguchi, C. Back, Y. Tokura, W. R. Branford, and

- H. Kurebayashi, Task-adaptive physical reservoir computing, *Nature Materials* (2023).
- [28] A. Khitun, Magnonic holographic devices for special type data processing, *Journal of Applied Physics* **113**, 164503 (2013).
- [29] A. Khitun, Parallel database search and prime factorization with magnonic holographic memory devices, *Journal of Applied Physics* **118**, 243905 (2015).
- [30] Á. Papp, W. Porod, and G. Csaba, Nanoscale neural network using non-linear spin-wave interference, *Nature Communications* **12** (2021).
- [31] D. V. Christensen, R. Dittmann, B. Linares-Barranco, A. Sebastian, M. Le Gallo, A. Redaelli, S. Slesazek, T. Mikolajick, S. Spiga, S. Menzel, I. Valov, G. Milano, C. Ricciardi, S.-J. Liang, F. Miao, M. Lanza, T. J. Quill, S. T. Keene, A. Salleo, J. Grollier, D. Marković, A. Mizrahi, P. Yao, J. J. Yang, G. Indiveri, J. P. Strachan, S. Datta, E. Vianello, A. Valentian, J. Feldmann, X. Li, W. H. P. Pernice, H. Bhaskaran, S. Furber, E. Neftci, F. Scherr, W. Maass, S. Ramaswamy, J. Tappson, P. Panda, Y. Kim, G. Tanaka, S. Thorpe, C. Bartolozzi, T. A. Cleland, C. Posch, S. Liu, G. Panuccio, M. Mahmud, A. N. Mazumder, M. Hosseini, T. Mohsenin, E. Donati, S. Tolu, R. Galeazzi, M. E. Christensen, S. Holm, D. Ielmini, and N. Pryds, 2022 roadmap on neuromorphic computing and engineering, *Neuromorphic Computing and Engineering* **2**, 022501 (2022).
- [32] I. Bertelli, J. J. Carmiggelt, T. Yu, B. G. Simon, C. C. Pothoven, G. E. W. Bauer, Y. M. Blanter, J. Aarts, and T. van der Sar, Magnetic resonance imaging of spin-wave transport and interference in a magnetic insulator, *Science Advances* **6**, eabd3556 (2020).
- [33] U. Makartsou, M. Golebiewski, U. Guzowska, A. Stognij, R. Gieniusz, and M. Krawczyk, Spin-wave self-imaging: Experimental and numerical demonstration of caustic and talbot-like diffraction patterns, *Applied Physics Letters* **124**, 10.1063/5.0195099 (2024).
- [34] V. Vlaminck, L. Temdie, V. Castel, M. B. Jungfleisch, D. Stoeffler, Y. Henry, and M. Bailleul, Spin wave diffraction model for perpendicularly magnetized films, *Journal of Applied Physics* **133**, 053903 (2023).
- [35] L. Temdie, V. Castel, M. Jungfleisch, R. Bernard, H. Majjad, D. Stoeffler, Y. Henry, M. Bailleul, and V. Vlaminck, Probing spin wave diffraction patterns of curved antennas, *Phys. Rev. Appl.* **21**, 014032 (2024).
- [36] B A Kalinikos and A N Slavin, Theory of dipole-exchange spin wave spectrum for ferromagnetic films with mixed exchange boundary conditions, *Journal of Physics C: Solid State Physics* **19**, 7013 (1986).
- [37] B. A. Kalinikos, Spectrum and linear excitation of spin waves in ferromagnetic films, *Soviet Physics Journal* **24**, 718 (1981).
- [38] B. A. Kalinikos and A. N. Slavin, Theory of dipole-exchange spin wave spectrum for ferromagnetic films with mixed exchange boundary conditions, *Journal of Physics C: Solid State Physics* **19**, 7013 (1986).
- [39] A. G. Gurevich and G. A. Melkov, *Magnetization Oscillations and Waves* (CRC Press, Boca Raton, FL, 1996).
- [40] L. Temdie, V. Castel, C. Dubs, G. Pradhan, J. Solano, H. Majjad, R. Bernard, Y. Henry, M. Bailleul, and V. Vlaminck, High wave vector non-reciprocal spin wave beams, *AIP Advances* **13**, 025207 (2023).
- [41] L. Temdie, V. Castel, T. Reimann, M. Lindner, C. Dubs, G. Pradhan, J. Solano, R. Bernard, H. Majjad, Y. Henry, M. Bailleul, and V. Vlaminck, Chiral excitation of exchange spin waves using gold nanowire grating, *Magnetochemistry* **9**, 199 (2023).
- [42] M. Kostylev, Non-reciprocity of dipole-exchange spin waves in thin ferromagnetic films, *Journal of Applied Physics* **113** (2013).
- [43] M. Haidar, M. Bailleul, M. Kostylev, and Y. Lao, Nonreciprocal oersted field contribution to the current-induced frequency shift of magnetostatic surface waves, *Physical Review B* **89** (2014).
- [44] T. Sebastian, K. Schultheiss, B. Obry, B. Hillebrands, and H. Schultheiss, Micro-focused brillouin light scattering: imaging spin waves at the nanoscale, *Frontiers in Physics* **3** (2015).
- [45] A. V. Chumak, V. I. Vasyuchka, A. A. Serga, and B. Hillibrands, *Nat. Phys.* **11**, 453 (2015).
- [46] G. Csaba, Á. Papp, and W. Porod, Perspectives of using spin waves for computing and signal processing, *Physics Letters A* **381**, 1471 (2017).
- [47] P. Pirro, V. I. Vasyuchka, A. A. Serga, and B. Hillibrands, *Advances in coherent magnonics*, *Nature Reviews Materials* **6**, 1114 (2021).
- [48] M. Benjamin Jungfleisch, Inelastic scattering of light by spin waves, in *Optomagnonic Structures*, Chap. 4, pp. 175–211.
- [49] A. Vansteenkiste, J. Leliaert, M. Dvornik, M. Helsen, F. Garcia-Sanchez, and B. Van Waeyenberge, The design and verification of MuMax3, *AIP Advances* **4**, 107133 (2014).